Proceedings of ASME Turbo Expo 2019: Turbomachinery Technical Conference and Exposition
GT2019
July 17-21, 2019, Phoenix, AZ, USA

GT2019-90927 DRAFT

VALIDATION OF LIFETIME MODELS FOR RECUPERATOR FOILS THROUGH LONG-TERM LABORATORY AND ENGINE TESTING

Sebastien Dryepondt
Oak Ridge National Laboratory
Oak Ridge, TN, USA

Bruce A. Pint
Oak Ridge National Laboratory
Oak Ridge, TN, USA

Robert Klug
Solar Turbines
San Diego, CA, USA

ABSTRACT

Reducing cost or enhancing efficiency are straightforward solutions to increase the market penetration of turbine-based combined heat and power (CHP) systems, and both could be achieved through materials development. For microturbine and small gas turbines the primary heat exchanger or recuperator is a key component for the turbine thermal efficiency, but also represents a significant cost (up to 40%). Recuperators are made of foil ~80-125 μm thick, and typical commercial materials include chromia-forming foils such as Haynes® HR120® (Fe-38Ni-25Cr), ATI's AL2025Nb (Fe-20Cr-25Ni-Nb) and alloy 625 (64Ni-23Cr-3Fe). Alumina-forming austenitic (AFA, Fe-25Ni-14Cr-3.5Al) foils exhibit good creep resistance and significantly better high temperature oxidation resistance in humid atmospheres in comparison with these chromia-forming alloys and could allow for a drastic increase of the turbine exhaust temperature, from ~650ºC up to ~750ºC-800ºC. ORNL is developing lifetime models based on the foil oxidation resistance to quantify the potential gains of switching from chromia to alumina forming alloys. If simple models can be used to describe the parabolic growth of alumina scale, more complex models based on para-linear growth kinetics need to be used for chromia forming alloys. This is because of the formation and volatilization of the oxy-hydroxide $CrO_2(OH)_2$ in H_2O-containing atmospheres. The volatilization rate varies from one alloy to another because it is quite sensitive to the oxide scale composition (Cr-rich scale + Mn, Ni and Fe oxides), which is a function of the alloy composition. ORNL has, therefore, used its extensive long-term oxidation database to determine the key lifetime model parameters i.e. the scale parabolic growth rate and volatilization rate as well as the Cr consumption with time. In addition, the volatilization rate is very sensitive to gas velocity. ORNL is, therefore, collaborating with Solar Turbines and Capstone to validate the models through the characterization of foils exposed to

actual engine tests, with some foils being tested for ~100,000h. Scanning electron microscopy was used to determine the foil microstructure and chemical evolution.

.

INTRODUCTION

Combined heat and power (CHP) is a type of distributed energy that can offer high efficiency (>80%) due to the recovery of waste heat to produce, for example, hot water or low pressure steam [1-3]. Reducing cost or enhancing efficiency are straightforward solutions to increase the market penetration of turbine-based CHP systems, and both could be achieved through materials development. A key component for the efficiency of small gas turbine and microturbine is the recuperator, because it uses the turbine exhaust gas to preheat the compressed air before entering the combustion chamber. To maximize the heat transfer, recuperators are composed of thin-walled metal foils made of alloys such as 120 (Fe-38Ni-25Cr), 2025Nb/709 (Fe-20Cr-25Ni-Nb) or 625 (64Ni-23Cr-3Fe)[4,5]. The high level of Cr and Ni in these alloys will result in the formation of thin Cr-rich scale in air, but, in H_2O containing atmospheres such as combustion environments, formation and volatilization of oxy-hydroxide ($CrO_2(OH)_2$) will result in ~linear consumption of Cr in the foil, thus limiting the foil lifetime [6-12].

A new class of alumina forming austenitic (AFA) steels have been developed at ORNL, with similar creep strength but better oxidation resistance than chromia-forming recuperator alloys [13-21]. In addition to slow growth rates, alumina scales are, indeed, very stable at high temperature in humid environments, and the Al consumption rate in AFA foils is expected to be minimal below 850ºC. In this paper, the oxidation behavior at 650ºC-800ºC in air+10%H_2O of various chromia-former and AFA foils is described. These data were used to develop oxidation-based lifetime models for recuperator foils, and validation of these models using field exposure is discussed.

EXPERIMENTAL PROCEDURE

Larger (1100 and 4500 kg) heats of AFA foils were produced for commercial processing to foil. The two foil batches characterized in this paper were 80 μm thick and ~21 cm wide (AFA-80) and 106 μm thick and ~39 cm wide (AFA-106). Two main microstructural differences between the two foils were noted. First, aluminum nitrides were present at the surface of AFA-106 due to insufficient cover gas during the foil heat treatments, and second, the AFA-106 foil exhibited a smaller grain size, ~5 to 10um versus ~50um for the AFA-80.
Commercial foils of 310, 709, 120 and 625 were received from vendors or industrial partners. The composition, thickness and grain size of the different foils are summarized in Table 1.

Table 1: Composition of the alloy in wt% measured by ICP spectroscopy, combustion and IGF analysis

Alloy	Cr	Ni	Al	Nb	Si	Other	Thickness (um)	Grain size(um)
120	24.7	37.6	0.1	0.6	0.2	0.2 Mo, 0.7Mn	88	23-28
310	24.1	19.5	0.01	0.01	0.33	1.7Mn, 0.15V	80	10
625	23.1	63.8	0.2	0.2	0.2	8.9Mo, 3Fe	125	12
709	20.3	24.7	0.05	0.2	0.4	1.5Mo, 1Mn	100 to 200	16
AFA-80*	14	25	3.5	2.5	0.2	2Mo, 2Mn	80	50
AFA-106*	14	25	3.5	2.5	0.2	2Mo, 2Mn	106	5 to 10

*Nominal composition. AFA foils contain 1W, 0.1C, 0.5Cu and 0.01B

Oxidation testing was conducted on foil coupons (~12mm x 18mm x ~80-200 μm) in the as-annealed surface condition after cleaning in acetone and methanol. 100h exposures were conducted in horizontal furnace at 650°, 700° and 800°C in air +10%Vol. H_2O with a flowing gas of 1.7-1.9 cm/s. The mass changes were measured after every cycle using a Mettler-Toledo model XP205 balance, with an accuracy of ~±0.01mg/cm^2. After exposure, selected specimens were Cu-plated and sectioned using conventional metallographic techniques for optical and scanning electron microscopy (SEM) observation as well as electron probe microanalysis (EPMA).

RESULTS

Laboratory Oxidation Testing

Figure 1 shows representative mass change curves for the 120, 310, 709, 625 and AFA foils exposed at 650ºC, 700ºC and 800ºC in air +10%H_2O. At all temperatures, the two AFA foils exhibited very limited mass gains after exposure for 15,000h. The behavior of the 310 and 625 foils was quite different with linear mass losses at 650ºC and 700ºC, due to the formation and volatilization of oxy-hydroxides ($CrO_2(OH)_2$) [6-9]. A final oxidation stage with no mass change was observed for some 310 coupons, after ~5,000h of exposure at 650ºC and 10,000h at 700ºC. The 120 and 709 foils showed more complex behaviors with several oxidation stages. At 650ºC, the 709 foils did not show any mass change for 2,000h, but then significant mass gains were observed, followed after ~ 4,000h by a new steady state stage for the specimen tested for 15,000h. At 700ºC, mass losses were first observed for the 709 foils, followed by rapid mass gains and, again, a final steady state stage after ~4,000h. One 709 foil was interrupted after 5,000h before a significant mass increase was observed (black arrow in Figure 1b). For the 120 foil tested at 650ºC, slight mass gains were first measured for 4,000h, followed by linear mass losses until the test was stopped after 20,000h of exposure. At 700ºC, the 120 foils exhibited linear mass losses, followed by significant mass gains during a few 100h cycles, and then a steady state stage. For one foil the mass increase was observed after ~4,000h while the mass increase was observed after ~10,000h for another 120 foil. The last 120 foil was still in the linear mass loss regime when it was stopped after 5,000h (black arrow in Figure 1b).

At 800ºC, all the chromia forming foils showed significant mass gains due to the formation of fast-growing Fe or Ni-rich oxides. One 120 foil exhibited limited mass change for 8,000h, while for the 625 foil, an acceleration of the mass losses was observed after 8,000h, partly due to scale volatilization but also because spallation took place at the foil edges.

Chemical maps for the 120 foil that was interrupted after 5,000h while still in the linear mass loss stage are shown in Figure 2. A thin (Cr,Mn)-rich scale can be observed at the foil surface, with oxide penetration along grain boundaries. In addition, Cr depleted and (Ni,Fe) enriched zones are visible beneath the oxide scale, above all in the grain boundary vicinity. Similar maps are presented in Figure 3 for the 120 foil tested for 20,000h at 700ºC. A much thicker bi-layer scale was observed, with a (Cr,Mn)-rich inner layer and a thick (Fe,Mn)-rich outer layer with the

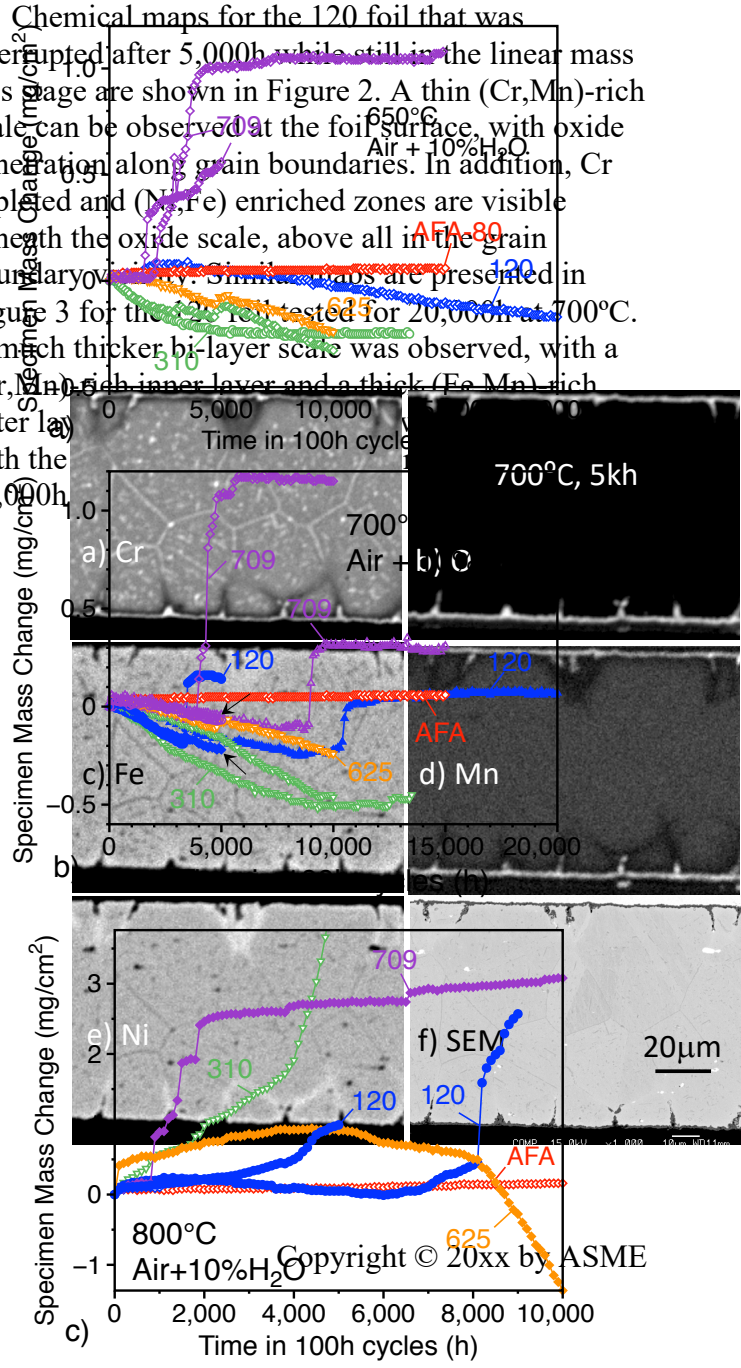

Figure 1. Mass change curves for the 310, 709, 2025Nb, 625 and AFA foils exposed in air+10%H_2O at a) 650ºC, b)700ºC and c)800ºC

Oxide penetration was o slightly deeper compared to the 5,000h foil exposure, and again a Cr-depleted zone was present beneath the scale. This change of scale morphology between the 5,000h and 20,000h exposure can be explained by the progressive decrease of the Cr concentration at the foil surface below the critical Cr concentration Cr_{cri} required for Cr-rich scale formation, leading to the sudden formation of fast growing Fe and Ni-rich oxides. The consumption of Fe and Ni to form these Fe and Ni-rich oxides will result in an increase of the Cr concentration at the foil surface above the Cr_{cri}, allowing the formation of a new Cr-rich scale below these Fe and Ni oxides.

Figure 2. Chemical mapping of one 120 foil exposed for 5,000h at 700ºC in air + 10%H_2O, a) Cr map, b) O map, c) Fe map, d) Mn map, e) Ni map and f) SEM micrograph

Finally, chemical maps for the 120 foil exposed in air+10%H_2O for 20,000h at 650ºC are shown in Figure 4.
A thin (Cr,Mn) oxide layer is present at the specimen surface, and, even if no sudden mass increase was observed during the 20,000h test (Figure 1a) many Fe-rich nodules grew atop the Cr-rich layer. Oxide penetration along grain boundaries and Cr-depleted zones were again observed beneath the scale.

Optical images of the 709 foils tested at 700ºC in air +10%H_2O for 5,000h and 10,000h are shown in Figure 5. As was observed for the 120 foil, a thin protective oxide layer was observed after 5,000h but a much thicker scale was observed after exposure for 10,000h.

Figure 3: Chemical mapping of 120 foil exposed for 20,000h at 700ºC in air + 10%H_2O, a) Cr map, b) O map, c) Fe map, d) Mn map, e) Ni map and f) SEM micrograph

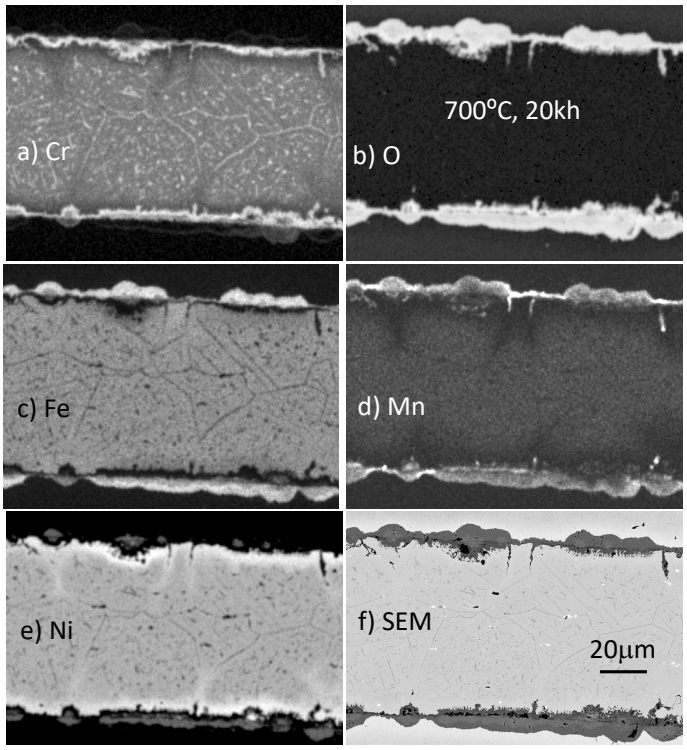

Figure 4: Chemical mapping of 120 foil exposed for 20,000h at 650ºC in air + 10%H_2O, a) Cr map, b) O map, c) Fe map, d) Mn map, e) Ni map and f) SEM micrograph

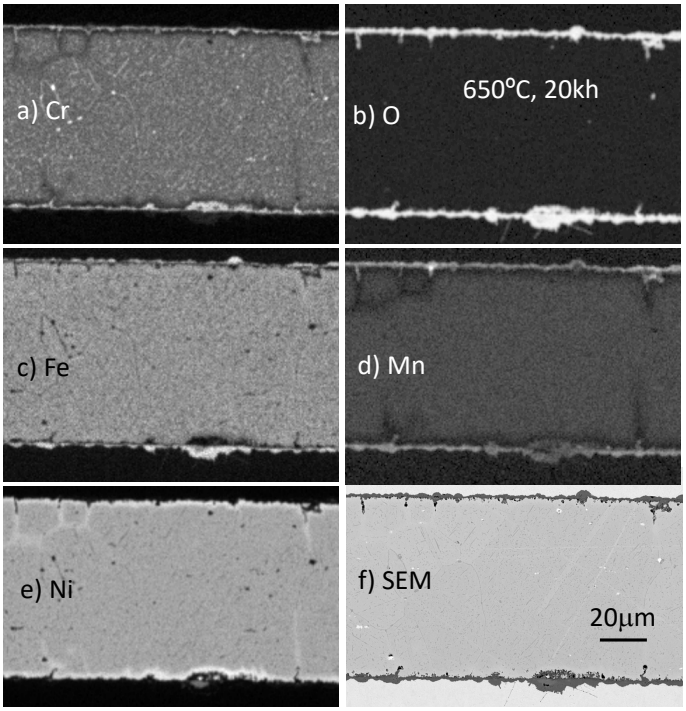

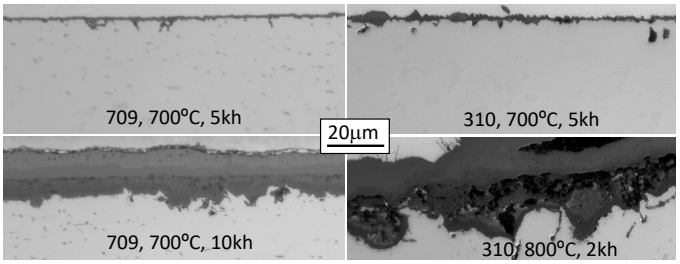

Figure 5: Cross-section optical micrographs of foils exposed in air+10%H_2O a) 709, 5,000h at 700ºC, b) 709, 10,000h at 700ºC, c) 310, 5,000h at 700ºC and d) 310, 2,000h at 800ºC

For the 310 foils, nodules started to form at the surface after 5,000h at 700ºC, and a massive oxide scale was formed at 800ºC after only 2,000h of exposure.

Figure 6 shows SEM pictures of the AFA-80 and AFA-106 foils after exposure for 15,000h at 650ºC, 700ºC and 800ºC. As expected from the mass gains, very thin oxide scales, less than 1µm thick, were observed at all temperatures. The scales grown on the AFA-80 and AFA-106 foils looked very similar which demonstrates that the formation of AlN precipitates in the AFA-106 foil during the foil processing heat treatment did not affect the growth of a protective Al-rich oxide scale.

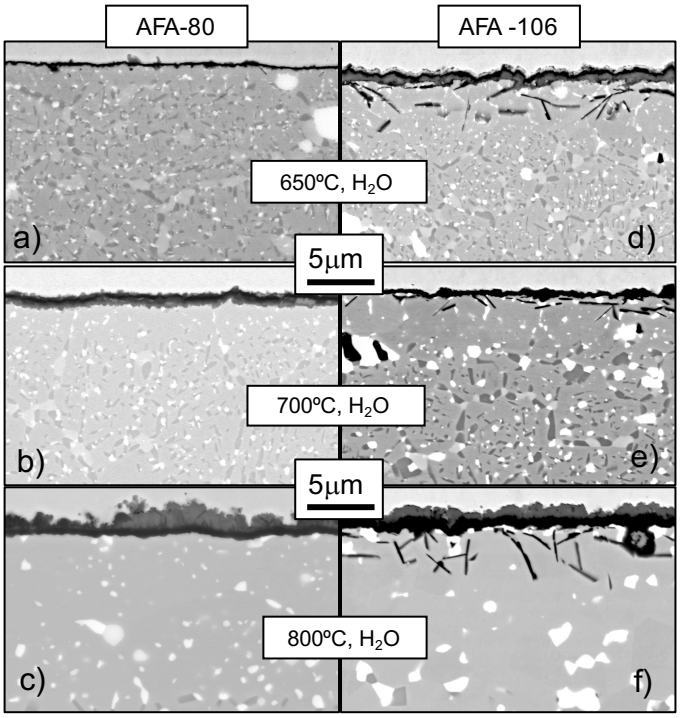

Figure 6: SEM micrographs of AFA foils exposed in air +10%H_2O for 15,000h at 650-800ºC, a)-c) AFA-80 foil, d)-f) AFA-106 foil

Foil lifetime modeling

Alumina scale

For alumina forming alloys, a stable scale is expected to form according to a simple parabolic law:

$$\frac{\Delta m}{A} = M_0 + \sqrt{k_p t} \qquad (1)$$

Where Δm is the mass change, A the coupon surface area, M_0 a fitting parameter to consider formation of transient oxides at the very beginning of the high temperature exposure, and k_p, the parabolic growth rate. Figure 7 shows the evolution of k_p wersus the inverse of temperature according to an Arrhenius law based on mass change data generated in air+10%H_2O for AFA foils, 80, 106 and 150µm thick. At 800ºC, a two-stage parabolic growth was observed, and the k_p values calculated during the second stage were consistent with values calculated from tests in air at 800ºC. Even if we consider only the k_p from the first oxidation stage at

800ºC, the Al consumption after 40,000h at 800ºC is only ~0.4mg/cm^2. For an 100µm thick foil, this leads to a decrease of the Al concentration in the foil from 3.5wt% to ~3wt%. The Al reservoir in AFA foil is, therefore, sufficient to ensure the formation of a protective alumina scale for duration much longer than 40,000h even at 800ºC.

Cr-rich scale

In humid environment, the formation and volatilization of the oxy-hydroxide $CrO_2(OH)_2$ will result in para-linear oxidation kinetic for chromia-forming foils due to the simultaneous parabolic growth and linear volatilization of the scale [6-9]:

$$\frac{dx}{dt} = \frac{\alpha^2 k_p}{2\rho^2 x} - \frac{k_l}{\rho} \qquad (2)$$

with x the scale thickness, ρ the scale density, α a parameter related to the scale composition, k_p the scale parabolic growth rate and k_l the linear volatilization rate from the surface.

One can assume that the scale growth rate k_p is the same in air and humid air. The evolutions of k_p versus temperature determined from long-term laboratory air tests are given in Figure 7 for alloy 709, 120 and 625. Even without considering scale volatilization, the scale growth rate is significantly slower for the AFA foils at T>700ºC compared to the chromia former foils.

Once k_p has been determined, they are at least four different methods to determine the volatilization rate k_l:

- (1) the gas transfer theory can be used to calculate the volatilization rate from the Cr_2O_3 scale based on the operating parameters such as the gas composition and velocity [9].
- (2) for laboratory tests, the mass gains data can be fitted with para-linear curves to determine k_l.
- (3) measurement of the scale thickness from cross section. Once the para-linear steady state stage is reached, i.e. the oxide scale thickness became nearly constant, the scale thickness X is simply given by: $X = k_p/k_l$
- (4) measurement of the Cr concentration in the entire foil after exposure. Cr consumption due to the growth and volatilization of the scale leads to a ~linear decrease of the Cr concentration in the foil.

Young and Pint have used with some success these different methods to determine k_l and Cr consumption in 709 foils exposed at 800ºC in air+10%H_2O for duration ranging from 1000h to 6000h [9]. All these methods work quite well when a pure oxide scale is formed, but, the oxide scales that form on commercial alloys are much more complex. First, as was shown in Figure 2, the Cr-rich scale often contains a significant amount of Mn. The volatilization rate of a $MnCr_2O_4$ spinel scale is lower than the volatilization rate of a Cr_2O_3 scale [6] and (Cr,Mn)-rich scales are likely to exhibited intermediate volatilization rates. The foils studied in this paper have Mn contents varying from ~0% for the 625 foil to 1.7% for the 310 foil, and the Mn concentration in the Cr-rich scale is expected to change significantly from one alloy to another.

In addition, the composition of the oxide scale varies with time with the progressive (310 and 625) or sudden (120 and 709) formation of Fe and Ni--rich nodules above the Cr-rich scale, leading with time to the formation of a dense outer (Fe,Ni)-rich layer. This scale is expected to have a low volatilization rate and could slow down Cr consumption. Measurement of the Cr content through the foil after exposure is the most reliable way to estimate foil lifetime, since the oxidation-based failure of the foil will be related to the Cr consumption during high temperature exposure. Figure 8 shows measurements of Cr loss for 120 foils exposed at 650 and 700ºC for up to 30,000h and 625 and 709 foils tested for up to 10,000h at the same temperature. Based on the 10,000h data, the difference between exposure at 650 and 700ºC is quite limited, and all the foils seem to show similar linear Cr consumption. Only the data generated for alloy 120 for duration up to 30,000h show a clear difference between the 650 and 700ºc exposures, highlighting the need for experimental long-term data to validate lifetime models.

<u>Long term engine tests</u>

Due to the difference in terms of gas velocity and composition, the foil volatilization rates can be quite different during microturbine operation and laboratory testing. Engine tests are, therefore, necessary to determine k_l and Cr consumption rate, and ORNL has conducted a 15,000h engine test with a 65kw capstone microturbine equipped with a rainbow recuperator made of AFA, 120 and 310 foils. The turbine exhaust temperature was increased to ~690ºC compared to ~633ºC in standard operation. The microturbine was disassembled by Capstone once the test was complete and the rainbow recuperator was recently shipped back to ORNL for microstructure characterization.

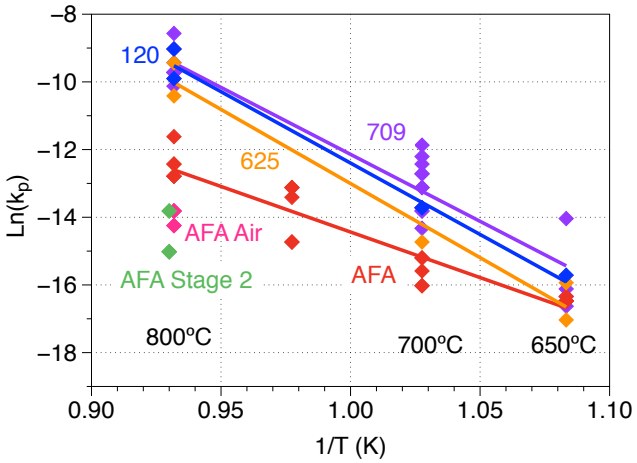

Figure 7: Arrhenius plot of the parabolic growth rate k_p based on oxidation data generated in air at 650-800ºC for AFA, 709, 120 and 625 foils

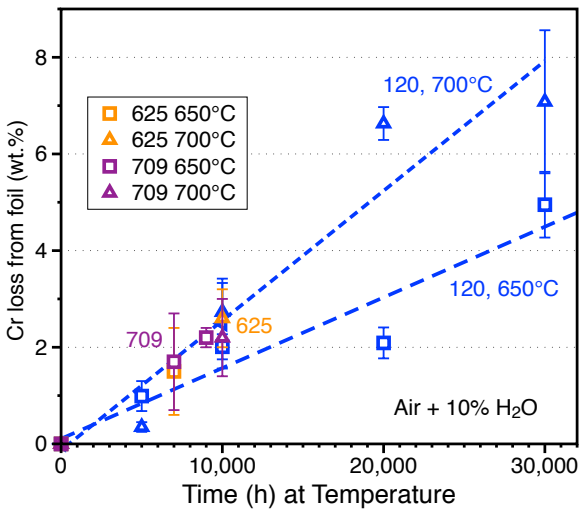

Figure 8: Cr loss from 709, 625 and 120 foils after exposure in air+10%H_2O at 650ºC and 700ºC measured by EPMA over the entire foil thickness

ORNL is also conducted microstructure characterization of AFA, 625 and 2025Nb (composition similar to 709) foil panels exposed in an engine test at Solar Turbines Inc. for duration ranging from 40kh to ~100 kh. Chemical maps of the oxide scale formed at the surface of the 625 panel is shown in Figure 9. A-bilayer oxide scale was observed with an outer (Ni,Fe)-rich layer and a Cr-rich inner layer with Al and Nb oxides incorporated into the inner scale. Si was detected in both layers but segregated preferentially at the outer scale/gas interface.

Similar maps for the scale grown at the surface of the 2025Nb are presented in Figure 10. A thinner bi-layer structure was observed, with Mn being detected in both scales but no Si. Al internal oxides and voids were also present beneath the Cr-rich inner layer, preferentially along grain boundaries. These differences between the 625 and 2025Nb foils highlights the importance of minor elements such as Mn and Si on scale formation and volatilization, and these mounted foils will be analyzed by EPMA to measure Cr profile and determine volatilization rates.

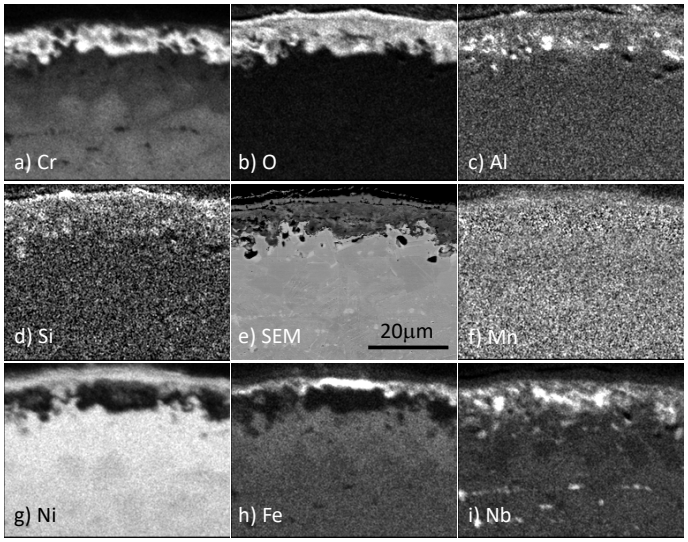

Figure 9: Chemical maps of the scale formed on a 625 foil after exposure in an engine test for 100000h at 643ºC, a) Cr, b) O, c) Al, d) Si, e) EM picture, f) Mn, g) Ni, h) Fe and i) Nb

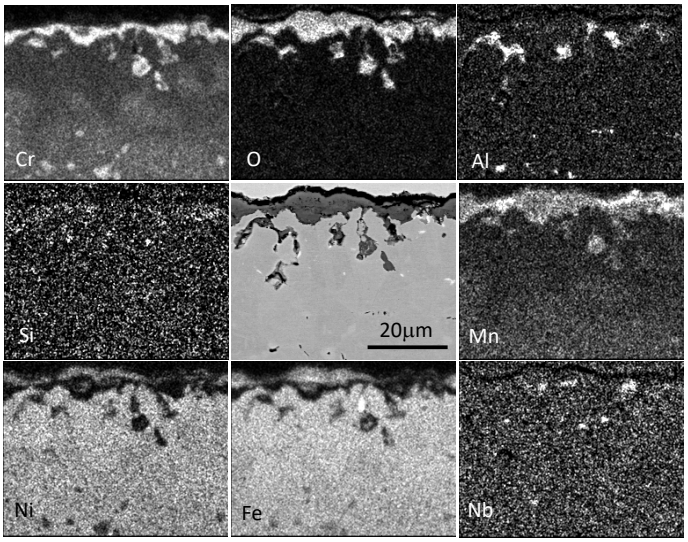

Figure 10: Chemical maps of the scale formed on a 2025Nb foil after exposure in an engine test for 100000h at 643ºC, a) Cr, b) O, c) Al, d) Si, e) EM picture, f) Mn, g) Ni, h) Fe and i) Nb

CONCLUSION

Long term oxidation data were generated at 650-800ºC for both chromia and alumina forming foils to develop oxidation-based lifetime models. Simple parabolic laws can be used to model the growth of alumina during high temperature exposure in air+10%H2O for AFA foils, and the very low growth rate indicate that these foils can be used in recuperator at temperature up to 800ºC. The situation is more complex for chromia forming foils due to the volatilization of Cr-rich scale in humid air, and lifetime models are based on para linear kinetics. The volatilization rate depends on many parameters such as the oxide scale composition and the gas flow rate, and characterization of foils exposed in the field is required to determine the Cr consumption rate and validate the lifetime models for chromia forming foils.

ACKNOWLEDGMENTS

The author would like to thank A. Willoughby, M. Stephens, J. Moser, T. Lowe and T. Jordan at ORNL for assistance with the experimental work. This research was sponsored by the U.S. Department of Energy, Office of Energy Efficiency and Renewable Energy, Advanced Manufacturing Office (Combined Heat and Power). This manuscript has been authored by UT-Battelle, LLC under Contract No. DE-AC05-00OR22725 with the U.S. Department of Energy. The United States Government retains and the publisher, by accepting the article for publication, acknowledges that the United States Government retains a non-exclusive, paid-up, irrevocable, world-wide license to publish or reproduce the published form of this manuscript, or allow others to do so, for United States Government purposes. The Department of Energy will provide public access to these results of federally sponsored research in accordance with the DOE Public Access Plan (http://energy.gov/downloads/doe-public-access-plan).

REFERENCES

1. Alanne, K. and Saari, A., 2004 “Sustainable Small-Scale CHP Technologies for Buildings: The Basis for Multi-

Perspective Decision-Making," Renewable and Sustainable. Energy Reviews, 8 , pp.401-31.
2. Kuhn, V., Klemes, J. and Bulatov, I., 2008 "MicroCHP:
Overview of Selected Technologies, Products and Field
Test Results," Applied Thermal Engineering 28 , pp.2039–2048.
3. Chicco, G. and Mancarella, P., 2009 "Distributed multigeneration: A comprehensive view," Renewable Sustainable Energy Rev. 13 , pp.535-551.
4. Matthews, W. J., More, K. L. and Walker, L. R., (2009)
"Comparison of Three Microturbine Primary Surface Recuperators," ASME Paper #GT2009-59041, presented at the International Gas Turbine & Aeroengine Congress & Exhibition, Orlando, FL, June, 8-12, 2009.
5. Bender, M. D. and Klug, R. C., 2014, "Comparison of Ni-Based 625 Alloy and ATI 20-25+Nb™ Stainless Steel Foils After Long-Term Exposure to Gas Turbine Engine Exhaust," ASME Paper #GT2014-25334, presented at the International Gas Turbine & Aeroengine Congress & Exhibition, Düsseldorf, Germany, June 16–20, 2014.
6. Asteman, H., Svensson, J.-E., Norell, M. and Johansson, L.-G., 2000, "Influence of Water Vapor and Flow Rate on the High-Temperature Oxidation of 304L; Effect of Chromium Oxide Hydroxide Evaporation," Oxidation of Metals, 54 , pp.11-26.
7. Opila, E. J., 2004, "Volatility of Common Protective Oxides in High-Temperature Water Vapor: Current Understanding and Unanswered Questions," Materials Science Forum, 461-464 , pp.765-74.
8. Pint, B.A., 2005, "The Effect of Water Vapor on Cr Depletion in Advanced Recuperator Alloys," ASME Paper #GT2005-68495, presented at the International Gas Turbine & Aeroengine Congress & Exhibition, Reno- Tahoe, NV, June 6-9, 2005.
9. Young, D. J. and Pint, B. A., 2006, "Chromium Volatilization Rates from Cr2 O3 Scales Into Flowing Gases Containing Water Vapor," Oxidation of Metals, 66 , pp.137-153.
10. Pint, B.A., 2006, "Stainless Steels with Improved Oxidation Resistance for Recuperators," Journal of Engineering for Gas Turbines & Power, 128 , pp.370-376.
11. Matthews, W. J., More, K. L. and Walker, L. R., 2007, "Accelerated Oxidation of Type 347 Stainless Steel Primary Surface Recuperators Operating Above 650°C," ASME Paper #GT2007-27916, presented at the International Gas Turbine & Aeroengine Congress & Exhibition, Montreal, Canada, May 14-17, 2007.
12. Pint, B. A., More, K. L., Trejo, R. and Lara-Curzio, E., 2008 "Comparison of Recuperator Alloy Degradation in Laboratory and Engine Testing," Journal of Engineering for Gas Turbines & Power, 130 (1), Art. No. 012101.
13 Yamamoto, Y., Brady, M. P., Lu, Z. P., Maziasz, P. J., Liu, C. T. Pint, B. A., More, K. L., Meyer, H. M. and Payzant, E. A., 2007, "Creep-Resistant, Al2 O3 -Forming Austenitic Stainless Steels," Science, 316 , pp.433-436.
14. Pint, B. A., Shingledecker, J. P., Brady, M. P. and Maziasz, P. J., 2007, "Alumina-Forming Austenitic Alloys for Advanced Recuperators," ASME Paper #GT2007-27916, presented at the International Gas Turbine & Aeroengine Congress & Exhibition, Montreal, Canada, May 14-17, 2007.
15. Brady, M. P., Yamamoto, Y., Santella, M. L., Maziasz, P. J., Pint, B. A., Liu, C. T., Lu, Z. P. and Bei, H., 2008, "The Development of Alumina-Forming Austenitic Stainless Steels for High-Temperature Structural Use," JOM, 60 (7), pp.12-18.
16. Pint, B. A., Brady, M. P., Yamamoto, Y., Santella, M. L., Maziasz, P. J. and Matthews, W. J., 2011, "Evaluation of Alumina-Forming Austenitic Foil for Advanced Recuperators," Journal of Engineering for Gas Turbines and Power, 133 , 102302.
17. Pint, B. A., Brady, M. P., Yamamoto, Y., Unocic, K. A. and Matthews, W. J., 2011, "Evaluation of Commercial Alumina-Forming Austenitic Foil for Advanced Recuperators,"

ASME Paper #GT2011-46704, presented at the International Gas Turbine & Aeroengine Congress & Exhibition, Vancouver, Canada, June, 6-10, 2011.

18. Pint, B. A., Dryepondt, S., Brady, M. P., Yamamoto, Y., 2013, "Evaluation of Commercial and Next Generation Alumina-Forming Austenitic Foil for Advanced Recuperators," ASME Paper #GT2013-94940, presented at the International Gas Turbine & Aeroengine Congress & Exhibition, San Antonio, TX, June, 3-7, 2013.
19. Yamamoto, Y., Santella, M. L., Brady, M. P., Bei, H. and Maziasz, P. J., 2009, "Effect of Alloying Additions on Phase Equilibria and Creep Resistance of Alumina-Forming Austenitic Stainless Steels," Metallurgical and Materials Transactions A, 40 , pp.1868-1880
Put text of Annex here
20. Pint, B. A., Dryepondt, S., Brady, M. P., Yamamoto, Y., 2013, "Evaluation of Commercial and Next Generation Alumina-Forming Austenitic Foil for Advanced Recuperators," ASME Paper #GT2013-94940, presented at the International Gas Turbine & Aeroengine Congress & Exhibition, San Antonio, TX, June, 3-7, 2013.
21. Pint B.A., Dryepondt S., Brady M.P., Yamamoto Y, Ruan B., McKeirnan R.D., 2015, "Field and Laboratory Evaluations of Commercial and Next Generation Alumina-Forming Austenitic Foil for Advanced Recuperators", ASME Paper #GT2015-42763, presented at the International Gas Turbine & Aeroengine Congress & Exhibition, Montreal, CA, June 15-19, 2015.

